Lipid-induced polymorphic amyloid fibril formation by α-synuclein

Horrocks Mathew (Orcid ID: 0000-0001-5495-5492)

RESEARCH ARTICLE

Protein Science
DOI10.1002/pro.4736

Lipid-induced polymorphic amyloid fibril formation by α-synuclein.

AUTHOR NAMES: Bhanu P Singh[1,3]*, Ryan J Morris[1], Tilo Kunath[2], Cait E MacPhee[1]*, and Mathew H Horrocks[3,4]*

AUTHOR ADDRESS:

1. School of Physics and Astronomy, The University of Edinburgh, Edinburgh, UK.

2. Centre for Regenerative Medicine, School of Biological Sciences, The University of Edinburgh, Edinburgh, UK.

3. EaStCHEM School of Chemistry, The University of Edinburgh, Edinburgh, UK.

4. IRR Chemistry Hub, Institute for Regeneration and Repair, The University of Edinburgh, Edinburgh, UK.

*Corresponding authors:

Bhanu P Singh. Email: Bhanu.Singh@ed.ac.uk

Cait E MacPhee. Email: Cait.Macphee@ed.ac.uk

Mathew H Horrocks. Email: Mathew.Horrocks@ed.ac.uk

KEYWORDS: Amyloid polymorphism, Lipid-Protein Interaction, α-synuclein, polypeptide self-assembly, protein aggregation

This article has been accepted for publication and undergone full peer review but has not been through the copyediting, typesetting, pagination and proofreading process which may lead to differences between this version and the Version of Record. Please cite this article as doi: 10.1002/pro.4736© 2023 The Protein Society
Received: Dec 02, 2022;Revised: Jun 27, 2023;Accepted: Jul 21, 2023

ABSTRACT

Many proteins that self-assemble into amyloid and amyloid-like fibres can adopt diverse polymorphic forms. These forms have been observed both *in vitro* and *in vivo* and can arise through variations in the steric-zipper interactions between □-sheets, variations in the arrangements between protofilaments, and differences in the number of protofilaments that make up a given fibre class. Different polymorphs arising from the same precursor molecule not only exhibit different levels of toxicity, but importantly can contribute to different disease conditions. However, the factors which contribute to formation of polymorphic forms of amyloid fibrils are not known. In this work, we show that in the presence of 1,2-dimyristoyl-sn-glycero-3-phospho-L-serine, a highly abundant lipid in the plasma membrane of neurons, the aggregation of α-synuclein is markedly accelerated and yields a diversity of polymorphic forms under identical experimental conditions. This morphological diversity includes thin and curly fibrils, helical ribbons, twisted ribbons, nanotubes, and flat sheets. Furthermore, the amyloid fibrils formed incorporate lipids into their structures, which corroborates the previous report of the presence of α-synuclein fibrils with high lipid content in Lewy bodies. Thus, the present study demonstrates that an interface, such as that provided by a lipid membrane, can not only modulate the kinetics of α-synuclein amyloid aggregation but also plays an important role in the formation of morphological variants by incorporating lipid molecules in the process of amyloid fibril formation.

INTRODUCTION

Protein self-assembly is involved in many diverse biological processes, from maintaining cellular homeostasis to being the causative mechanism of many diseases. Some well-known examples of nature utilising self-assembled protein structures are the cytoskeletal architectures built from actin and tubulin[1,2], the aggregation of blood fibrinogen into fibrin[3], the formation of collagen fibres[4], and the synthesis of spider silk[5] to name but a few. Under the appropriate conditions, however, many proteins can self-assemble into supramolecular structures known as amyloid fibrils that are associated with more than thirty human diseases including Parkinson's and Alzheimer's disease[6]. Despite their prominent role in disease, amyloid fibril structures have been successfully utilized in the field of nanotechnology, bioelectronics, biomedicine and material science due to their exceptional mechanical properties[7,8]. Thus,

understanding the factors that control and modulate the processes of protein self-assembly is of fundamental importance and will impact multiple areas of current scientific research.

Amyloid fibril formation has been reported for a large number of proteins, including many that are not known to form amyloid fibrils *in vivo*[9]. Although these amyloid fibril forming proteins are distinctly different in primary amino acid sequence[10], the shared structural features are strikingly similar. Studies carried out by solid-state NMR, cryo-EM and diffraction methods[10,11] have enriched our knowledge of the common structural elements of amyloid fibrils. These studies show that amyloid fibrils consist of orderly arrangements of □-sheets and □-strands that are organized parallel and perpendicular to the fibril axis, respectively. Each □-sheet interacts with a neighbouring sheet via "steric-zipper" interactions between amino acid sidechains[12]. Interestingly, it was observed in multiple amyloid fibril forming systems that the β-sheets can pack via different symmetry classes of steric-zipper interactions[13,14], which results in different conformational variants known as polymorphs. Another factor which can contribute to amyloid fibril polymorphism is the differential packing of protofilaments into mature fibrils, which arises due to differences in lateral contacts between protofilaments[15]. For example, a cryo-EM study of two different polymorphs of tau fibrils (paired helical and straight fibrils) extracted from an Alzheimer's disease *post-mortem* brain tissue show that these variants have two identical protofilaments but have differential packing arrangement of protofilaments[16]. Similarly, cryo-EM structure of full-length α-syn and a C-terminally truncated form of α-syn (1-121) show both consist of two protofilaments with diameter of 10 nm. However, full length α-syn forms a left-handed helix, whereas a C-terminus truncated α-syn shows a right-handed helix. Furthermore, the helical rise and twist angle of two structure are also different[17,18]. Such polymorphs have been observed under both *in vitro* and *in vivo* conditions for various proteins. Several studies investigating pathologically relevant amyloid fibrils have reported the presence of polymorphic forms, and this phenomenon is emerging as a common feature for amyloid fibre forming proteins[13,19,20], however, it is not known if this phenomenon extends to functional amyloids.

Apart from the different steric-zipper interactions that can occur between the □-sheets of a protofibril and the differential packing arrangements of protofilaments into mature fibrils, another factor that contributes to the observed polymorphism is the number of protofilaments that make up the mature fibril[21]. The polymorphic forms of these fibrils possess interesting

geometrical features such as helical and twisted architectures, variable widths (10 - 173nm), and higher persistence lengths which are directly correlated with the protofibril number[22,23].

Importantly, different polymorphs arising from the same precursor protein exhibit varying levels of toxicity and disease conditions[20,24]. For example, amyloid fibrils isolated from brain cells of Alzheimer's patients have been found to be morphologically homogenous in a single patient but different from one patient to another[25], and the varying polymorphs of these fibrils formed by the □-amyloid protein display altered levels of toxicity in neuronal cells[26]. In addition to differences in cell toxicity in a single cell line, amyloid fibril polymorphs can also target different tissues and cell lines resulting in distinctive pathologies[27]. In the case of synucleinopathies (e.g. Parkinson's disease, multiple system atrophy, dementia with Lewy bodies), these conditions are all associated with the formation of α-syn amyloid fibrils[28]. However, the amyloid fibril structures presented in these pathologies are different[24], i.e. these diseases are correlated with different polymorphic forms of α-syn amyloid fibrils. Additionally, one study showed that injecting different strains of α-syn fibrils into rat brains resulted in varying forms of synucleinopathies, with fibrils causing Parkinson's disease and ribbons causing Lewy body dementia.[29]. Thus, it is important to understand and discover the factors that play an important role in the formation of fibril polymorphs.

α-Syn is a small, 140 amino acid protein present in the presynaptic termini of neuronal cells. In its soluble form, it presents as an intrinsically disordered protein, whereas in its membrane-bound form, the N-terminal region acquires an a-helical rich structure[30]. Its membrane-bound form has been linked to its putative physiological role in synaptic plasticity, neurotransmitter release, assembly and disassembly of the SNARE complex[31]. Interestingly, a recent study showed the importance of native α-syn in the central nervous system for providing innate immunity against RNA virus infection[32]. Importantly, many *in vitro* studies have shown that its interaction with different lipid membranes plays an important role in modulating the kinetics of amyloid fibril formation[30].

The lipid composition of the brain changes with age[33] and PD is largely an age-associated pathological condition[34]. Phosphatidylserine in one of the most abundant lipids in synaptic vesicles[35], and importantly, it has been shown previously that phosphatidyl serine synthase has an elevated activity in the substantia nigra of patients with Parkinson's disease[36]. To investigate the effect of this on α-syn, we have used the synthetic lipid 1,2-dimyristoyl-sn-glycero-3-phospho-L-serine (DMPS), and have shown that it can trigger the conformational changes of

α-syn into a range of structures. Their morphologies include thin and curly fibrils, helical ribbons, twisted ribbons, nanotubes, and flat sheets. Further analysis of the fibril characteristics shows a large variation of polymorphs within each class; such a high number and different class of amyloid polymorphs under a single set of environmental condition has hitherto not been reported for any protein system. Finally, using single-molecule total internal reflection fluorescence (TIRF) microscopy with single aggregate visualization by enhancement (SAVE) imaging[37], we show evidence for the incorporation of lipid molecules into mature amyloid fibrils. Thus, this study shows that the presence of DMPS not only modulates the kinetics and polymorphic nature of α-syn amyloid formation, but also can be integrated into the mature fibrils.

RESULTS

In the presence of DMPS vesicles, folding of α-syn follows a two-state transition

It is well established that in the presence of interfaces such as anionic lipids, cardiolipin, poly unsaturated fatty acids, detergent and trifluoroethanol, the secondary structure of α-syn changes from random coil to an α-helical form[30]. Although the structural and conformational dynamics of membrane-bound and non-aggregated states of α-syn have been well characterized[38], it is not fully understood if the membrane-bound protein molecules are on the aggregation pathway. Importantly, a study carried out in the presence of sodium dodecyl sulfate (SDS) micelles – a well characterized phospholipid mimetic – had shown that α-syn can adopt three well-defined equilibrium states (unfolded, high degree of α-helical structure, and an intermediate state), depending upon the micelle concentration[39]. Similarly, in the presence of organic solvents such as simple and fluorinated alcohol, a multiphasic structural transition of α-syn has been observed[40,41]. Furthermore, the observed transition phases differed between solvents. A common feature for these studies, however, is that all were characterized by the presence of a partially folded intermediate at a relatively low concentration. Importantly, these intermediate species were found to increase the propensity for α-syn to aggregate. To understand if a helical intermediate is involved in the fibril-formation of α-syn in the presence of DMPS vesicles, we have employed the phase diagram method of Kuznetsova *et al.*[42], using the data obtained from circular dichroism (CD) spectroscopy at different DMPS/α-syn molar ratios from a value 0 to 30. In the absence of DMPS vesicles, CD spectra were flat except for minimum at ~198 nm,

which is characteristic of a random coil configuration. As we increased the ratio of DMPS/α-syn, we observed a significant change in the CD spectra. Minima appeared at values of 222 and 208 nm which is indicative of the formation of an α-helical conformation **(Fig. 1A)**. A plot of ellipticity at 198 nm (θ_{198}) against the ellipticity at 222 nm (θ_{222}) shows a linear trend across all lipid/protein molar ratios **(L/P) (Fig. 1B)**. It is important to note that α-syn shows a remarkable ability to adopt a range of structural architectures by involving different lengths of its N-terminus region (corresponding to residue 1 to ~ 100) to undergo structural transition[43–47]. Studies carried out in the presence of other interfaces show the different lengths of the N-terminus of the α-syn fold into helical structure depending upon the interface:protein ratio. When the interface:α-syn ratio is low, only a partial region of the N-terminus of α-syn adopts a helical structure, whereas at higher interface:α-syn ratios, the complete N-terminus region of α-syn adopts an α-helical structure. If that were the case with the interface provided by DMPS, we would have observed a transition point in the phase diagram. A linear trend across all the points in the phase diagram suggests α-helical content of α-syn does not change with DMPS:α-syn ratios. This result clearly shows that in the presence of DMPS vesicles, α-syn follows a two-step folding pathway and does not form a helical intermediate, i.e. upon interaction with DMPS vesicles, α-syn acquires the α-helical structure which does not change with L/P ratio. Furthermore, the presence of a single isochromatic point on far-UV CD spectra is a characteristic of the two-state folding model of protein folding[48]. The fact that isochromatic points were observed at 203 nm for all CD spectra at different L/P ratios in our experiments provides further evidence for the validity of the two-state model in describing α-syn folding on the surface of DMPS vesicles. This is in contrast to the previously reported multiphasic folding of α-syn on the interface of SDS micelle and organic solvent. It is also important to note that the results presented here are physiologically more relevant compared to similar studies with SDS micelles or organic solvents since DMPS is one of the most abundant components of synaptic vesicle membranes[35] and its elevated level has been linked to PD[36].

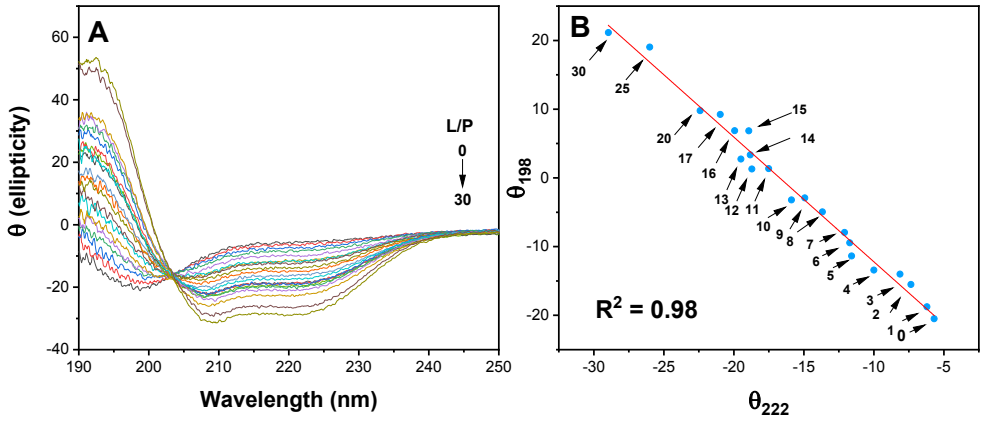

Figure 1. CD Spectroscopy (A) Far-UV CD spectra of 10 μM α-syn alone and in presence of 10, 20, 30, 40, 50, 60, 70, 80, 90, 100, 110, 120, 130, 140, 150, 160, 170, 200, 250 and 300 mM DMPS vesicles at 30 °C. **(B)** Plot of ellipticity at 222 nm (θ_{222}) against ellipticity at 198 nm (θ_{198}), the numbers denote the lipid/protein ratio across different points. . All the spectra were acquired in the 25 mM phosphate buffer at pH 7.4 and 30 °C.

Lipid to protein ratio modulates the kinetics of α-syn aggregation

To investigate the effect of L/P molar ratio on α-syn aggregation, we incubated the recombinantly expressed monomeric α-syn at L/P ratios of 0.5, 1, 2, 4 and 8. We detected aggregate formation using the amyloid-binding dye thioflavin-T (ThT) **(Fig. S1A-E)**. To confirm that the ThT signal was not affected by lipid vesicles or buffer alone, we incubated vesicles and buffer without protein. We did not observe any change in the ThT signal during the entire incubation period for either sample **(Fig. S1F)**. It was previously demonstrated that the presence of salt reduces the ionic interaction between anionic head group of lipid and positively charged N-terminus of the α-syn[35]. However, it is also known that under physiological conditions, α-syn exist in soluble and membrane-bound form[31]. Therefore, we avoided using salt in our experiments to investigate the effect of membrane binding on amyloid fibril formation by α-syn.

In the presence of DMPS vesicles, the lag-time of fibril-formation was dependent on the L/P ratio; an increase in this ratio led to a significant decrease in the lag-time (**Fig. 2**). Despite the significance, it is evident that there is a high variability in the lag-phase for each ratio. The mechanistic details for lag-time variability are not well understood, however, the stochastic nature of nucleation at the molecular level may influence the observed variability at the macroscopic scale[49]. Indeed, α-syn is known to exhibit highly variable self-assembly kinetics

between replicates of the same sample[50]. These data imply that DMPS vesicles significantly promotes the fibrillization of α-syn, but does not affect the lag-time variability of protein fibrillization.

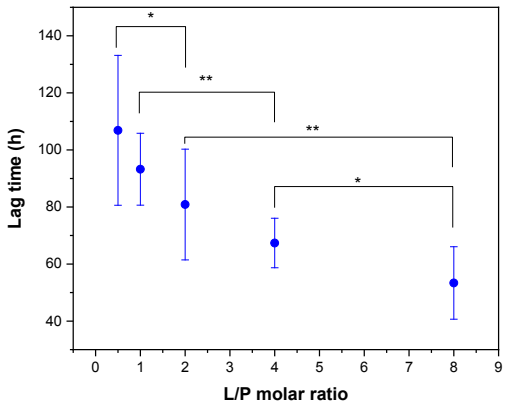

Figure 2. The lag-time of fibril-formation is affected by lipid:protein ratio. Plot of lipid:protein molar ratio against the lag-time of α-syn amyloid formation in the presence of DMPS vesicles (mean ± S.D., n = 8). Lag time was calculated the time at which the fluorescence intensity reached 10% of that at the plateau phase. A statistical analysis of data in this figure shows that there are significant differences between the groups. This was determined by analysis of variance, which found that p-values for *p < 0.05 and **p < 0.005.

In the presence of DMPS vesicles, α-syn aggregates into many distinct polymorphs

We next used transmission electron microscopy (TEM) to study the effect of DMPS vesicles on the morphology of aggregates formed. In our initial experiment, we used a 50 μM concentration of α-syn and an L/P ratio of 8 to minimize the lag time of the reaction[35]. We then compared the morphological structures that were formed in the presence of DMPS vesicles to the fibrils formed in the absence of lipid vesicles. In the absence of DMPS vesicles, we observed only a slight increase in the ThT signal at the same protein concentration. However, when we increased the protein concentration to 100 μM, a significant increase in signal was observed **(Fig. S2A)**. The kinetics of α-syn fibril-formation in the presence of DMPS, which was used for TEM studies, are shown in **Fig. S2B**. In the absence of DMPS vesicles, we identified small oligomeric aggregates when α-syn was incubated at a concentration of 50 μM (**Fig. 3A**). However, at a higher concentration of 100 mM, we observed fibrils with a rod-like morphology (**Fig. 3B-C**). In contrast, TEM images of amyloid fibrils of α-syn formed in the presence of the DMPS vesicles exhibited a large diversity of morphologies (**Fig. 3D–L**), including thin and curly amyloid fibrils without any clear periodicity (**Fig. 3D-F**), helical ribbons (**Fig. 3G-I**) and twisted ribbons (**Fig. 3J-L**). These morphologies were the predominant structures observed, but we also found the presence of nanotubes (**Fig. 4A**), and flat sheets

(**Fig. 4B**). While thin and curly amyloid fibrils appear to be the earliest stable fibril form, the other forms appear to be generated by the high-order association of thin and curly amyloid fibrils. The characteristic feature of twisted ribbons is the presence of an anisotropic cross section and saddle-like (Gaussian) curvature, whereas helical ribbons can be wrapped around a hypothetical cylinder of a finite radius and characterized by defined mean curvature associated with bending, but with zero Gaussian curvature[21,51]. Although twisted and helical ribbons both contain multiple protofilaments, the transition from twisted ribbons to helical ribbons takes place when the number of protofilaments reaches a critical number (parameterized by the width to thickness ratio). When this ratio is low, twisted polymorphs are energetically more favoured, whereas at high ratios helical polymorphs are energetically more stable[51]. Further, helical ribbons can transform into nanotubes, which is a consequence of eliminating line tension associated with the exterior protofilaments of a fibril[51]. Flat sheets can form by the assembly of multiple parallel protofilaments and these structures have a higher stiffness than helical ribbons[52].

These results clearly demonstrate that in the presence of DMPS vesicles, α-syn aggregates into diverse polymorphic forms. Compared to previous data, the presence of such a large number of polymorphic variants formed under identical environmental conditions has not been reported before for any protein. It was previously reported that in the presence of phospholipid vesicles composed of 1,2-dipalmitoyl-sn- glycero-3-phosphate (PA) and 1,2-dipalmitoyl-sn-glycero-3-phospho-choline (PC), there was no effect on the morphology of the fibrils as compared to in the absence of these vesicles[53]. In a recent cryo-EM study by Benedikt *et al*., three dominant protofilament folds were observed when α-syn was aggregated in the presence of POPA/POPC lipid vesicles[54]. With differential quaternary arrangements, these protofilament resulted in six polymorphs of α-syn. However, unlike our approach described here, the study involved subjecting the samples to repeated cycles of sonication for 20-48 hours before incubating it for aggregation reaction under mechanical shaking. Surprisingly, in the presence of small unilamellar vesicles composed of DMPS or DLPS, α-syn has been shown to form only thin and curly amyloid fibrils with an absence of any higher order aggregates[35,55]. One explanation for these differences is that they incubated α-syn and lipids at pH 6.4 in a phosphate buffer[35]. The presence of phosphate in the reaction solution in addition to variations in pH has been reported to have a strong effect on amyloid fibril morphology[56,57], which can cause proteins to adopt entirely different conformations, resulting in different polymorphs[58]. Our observation of a large spectrum of polymorphic forms of amyloid fibrils formed in the presence of DMPS differs

from previous report. All things considered, it appears that many factors, including lipid:protein ratio, the chemistry of the lipid head group and solution conditions (e.g., pH and co-solutes) can influence the formation of polymorphic forms of α-syn fibrils.

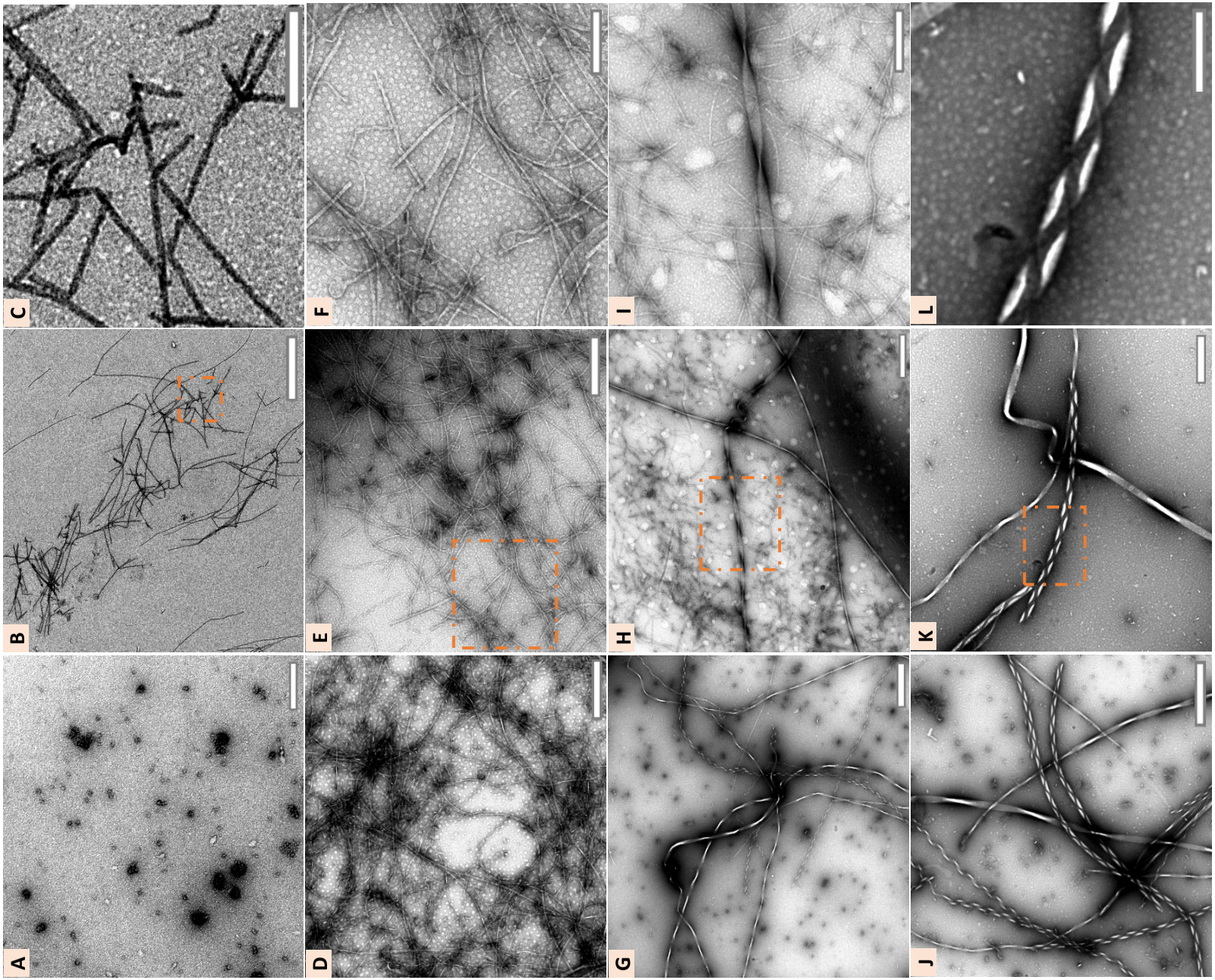

Figure 3. TEM imaging. Polymorphs of α-syn (50 μM, 100 μM) in the absence and presence of DMPS vesicles (400 μM)**. (A)** 50 μM of α-syn in absence of DMPS vesicles shows formation of small oligomers. **(B-C)** 100 μM of α-syn in the absence of DMPS vesicles shows presence of straight rod-like fibrils. In the presence of DMPS vesicles α-syn (50 μM) forms **(D-F)** thin and curly amyloid fibrils **(G-I)** helical ribbons and **(J-L)** twisted ribbon. Images show gross morphological features; note the variation in scale bar across images. Scale bar is 0.3 μm (A), 1 μm (B, G, J and H), 0.5 μm (D, E and K), 0.2 μm (C, F and L) and 0.4 μm (I). Images C, F, I and J are from area shown within rectangle in B, E, H and K, respectively.

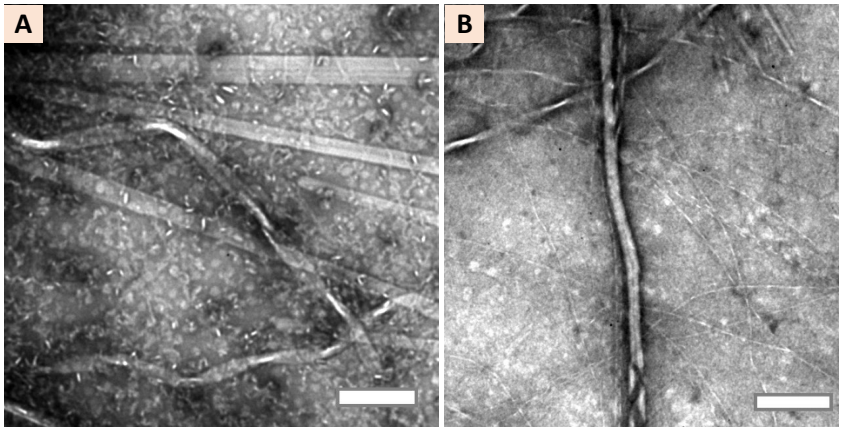

Figure 4. TEM imaging. Minor morphological variants **(A)** Flat sheets and **(B)** Nano-tube structure. Scale bar is 0.2 μm in figure A, and 1 μm in figure B.

Impact of L/P ratios on fibril morphology.

To further investigate the impact of L/P ratios on fibril morphology, we performed TEM imaging at L/P ratios of 1, 2, and 4. Our observations revealed distinct structural characteristics at different L/P ratios. At an L/P ratio 1, only thin and curly fibrils were formed. These fibrils were also found to be laterally associated at several instances, resembling the morphology of helical ribbons. However, unlike helical ribbons at L/P ratio 8, cross over of the individual fibrils were observed at this ratio **(Fig. 5A-C)**. At an L/P ratio 2, we observed that all of the fibrils exhibited small spherical structures along their length. Similar to the L/P ratio of 1, clusters of laterally associated mature fibrils resembling helical ribbons structures were also observed **(Fig. 5D-F)**. At an L/P ratio 4, the predominant form of fibrils displayed loop structures along their length and also at their ends **(Fig. 5G)**. Upon closer examination, these

fibrils consisted of two closely associated mature fibrils with an average distance of 9 nm (indicated by red arrows in **Fig. 5H**), and occasionally separated by significant gaps, forming the observed loop structures **(**indicated by blue arrows in **Fig. 5H)**. Furthermore, the helical ribbon structures formed at this L/P ratio showed a smooth surface with very little pronounced individual fibrils structures **(Fig. 5I)**. No other morphological structures were observed at any of these L/P ratios (1, 2, and 4).

The observed differences in fibril structures at various L/P ratios may be attributed to the presence of lipid molecules which were co-localized with the fibril (see **Fig. 9**). Benedict *et al*. also found that hydrophobic residues on the fibril surface were coated with lipid molecules[54]. In our experiment, the absence of spherical or loop structures at an L/P ratio of 1 suggests that there may not be enough lipid molecules to coat these surfaces effectively. In contrast, at an L/P ratio of 8, there are sufficient lipid molecules present, which adequately cover these surfaces. Additionally, the presence of lipid-coated fibrils will facilitate their lateral association to minimize the exposure of their hydrophobic surfaces. This would promote the fibrils to form hierarchical aggregates, as observed at L/P ratio of 8.

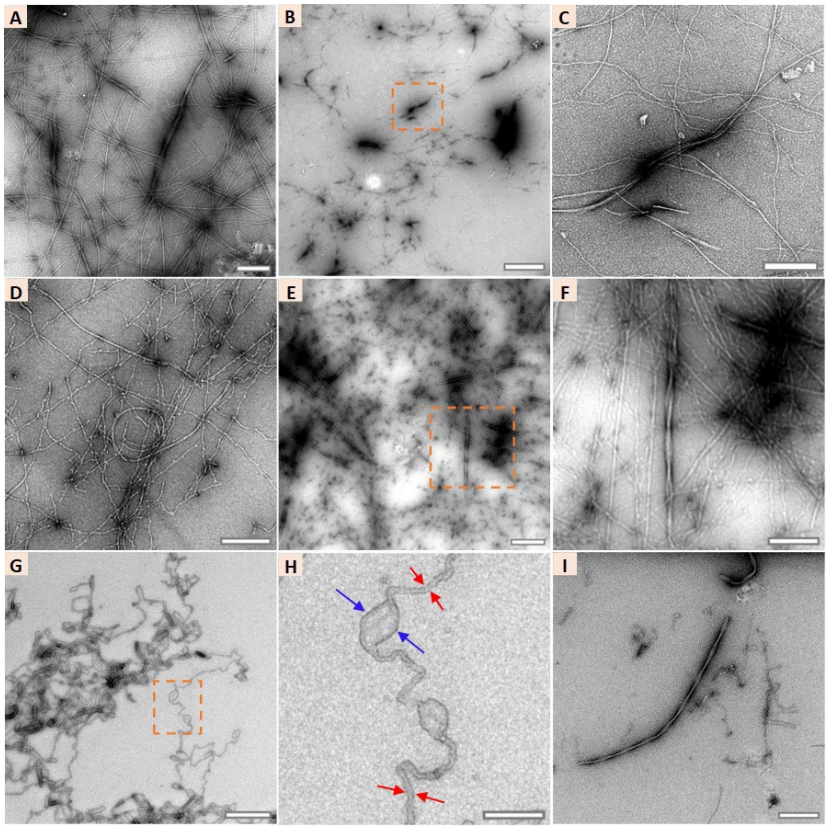

Figure 5. TEM images of α-syn fibrils at varying L/P ratios. The effect of L/P ratio on the morphology of α-syn fibrils. **(A-C)** Fibrils formed at L/P ratio 1 exhibit thin and curly fibrils,

with instances of mature fibril clustering. **(D-F)** Fibrils formed at L/P ratio 2 display small spherical structures along their length with instances of mature fibrils clustering **(G-I)** Fibrils formed at L/P ratio 4 show closely associated two mature fibrils along their length (indicated by red arrows in **Fig. H**), forming loop structures (indicated by blue arrow in **Fig. H**), and the presence of twisted ribbon structures in **Fig. I**. Scale bars: 0.1 μm (H), 0.3 μm (G), 0.5 μm (A, C, D, and F), 1 μm (E), and 2 μm (B). Image C, F, and H correspond to the areas under the brackets in images B, E, and G, respectively.

Quantitative analysis of amyloid fibrils

As the morphology of α-syn fibrils in the presence of an L/P ratio of 8 contained several distinct morphological features from those in the absence of DMPS vesicles and other L/P ratios we examined, we performed quantitative analysis of TEM images to extract the structural characteristics (e.g., length, width) of the polymorphic fibrils. To this end, we measured the width and contour length of 900 and 1200 fibrils, respectively, formed in both the absence of lipid vesicles and at the L/P ratio 8. A comparison of fibril length and width is shown in **Fig. 6**.

The results obtained from this analysis show that at the L/P ratio 8, the average fibril length is 10.8 ± 7.5 μm with a minimum and maximum value of 0.8 and 43.2 μm, respectively. In comparison, fibrils formed in the absence of DMPS were measured to have an average length of 2.6 ± 2.6 μm with a minimum and a maximum length of 0.2 and 15.8 μm, respectively (**Fig. 6A**). Thus, fibrils formed at the L/P ratio 8 are much longer compared to those that were formed in its absence. Moreover, such long fibril lengths have not, to the best of our knowledge, been previously reported for α-syn. Analysis of fibril width shows that at the L/P ratio 8, the average width is 30.4 nm with a minimum and maximum of 3 and 157 nm, respectively. On the other hand, fibrils formed in the absence of DMPS vesicles have an average width of 16.3 nm, with a minimum and maximum value of 7 and 33 nm, respectively (**Fig. 6B**). Further, we performed a quantitative analysis to understand the relative distribution of fibrils under each category (**Fig. 6C**). For this we analysed total 637 fibrils which revealed highest abundance of thin and curly amyloid fibrils (78.96 %), followed by twisted ribbons (13.81%), helical ribbons (5.02%), flat-sheet (1.41%) and nano-tubes (0.78%).

For fibrils formed in the absence of DMPS, the width of the fibril remains constant for its entire length. In contrast, the width of fibrils generated in the presence of DMPS shows a constant width for thin and curly fibrils and for flat sheets. However, helical and twisted ribbons possess a periodic modulation in the width as a function of fibril length. It has been demonstrated that shorter peptides have a higher tendency than larger proteins to form larger fibril assemblies consisting of laminated b-sheets which arise from the lateral association of protofibrils[59]. Most studies that report the presence of amyloid fibril polymorphs that are comprised of a large numbers of protofibrils have typically been studied in short-peptide systems - either synthetic peptides or fragments of amyloid forming proteins[14,15,52,60–64]. The major drawback of studying small peptides is that in these studies, fibril-formation occurs via homotypic-interactions[14]. In contrast, structural studies of full-length fibrils at atomic length scales show these interactions are composed of 25-70 residue heterotypic interactions[16,65,66]. For example, the 11-aa peptide of the NAC region of α-syn makes a homotypic steric zipper structure, whereas the same region in the full-length protein bends twice and form an S-shaped heterotypic zipper[66,67]. Although many full-length proteins have been shown to form polymorphic forms, the number of protofibrils involved in these polymorphs is limited to only a few[13,17,56,66,68–70]. Apart from α-syn, only □-lactoglobulin and lysozyme have been reported to form higher order polymorphic assemblies of full-length protein. For lysozyme it was shown to form both helical and twisted ribbons whereas □-lactoglobulin can only form helical fibrils[22,68]. For polymorphs consisting of high numbers of protofibrils, it was found that these fibrils were intrinsically unstable and degrade into smaller fragments. The studies in these structures were observed were performed at low pH (2) and high temperature (90 °C); at lower temperatures the same proteins are unable to form higher-order assemblies of protofibrils. The findings described here demonstrate the existence of a large spectrum of polymorphic forms of amyloid fibrils produced at more physiological conditions (both temperature and pH). The fibrils we observe vary widely in their physical characteristics and importantly, are highly stable (**Fig. 3, 4, 8 and S4**).

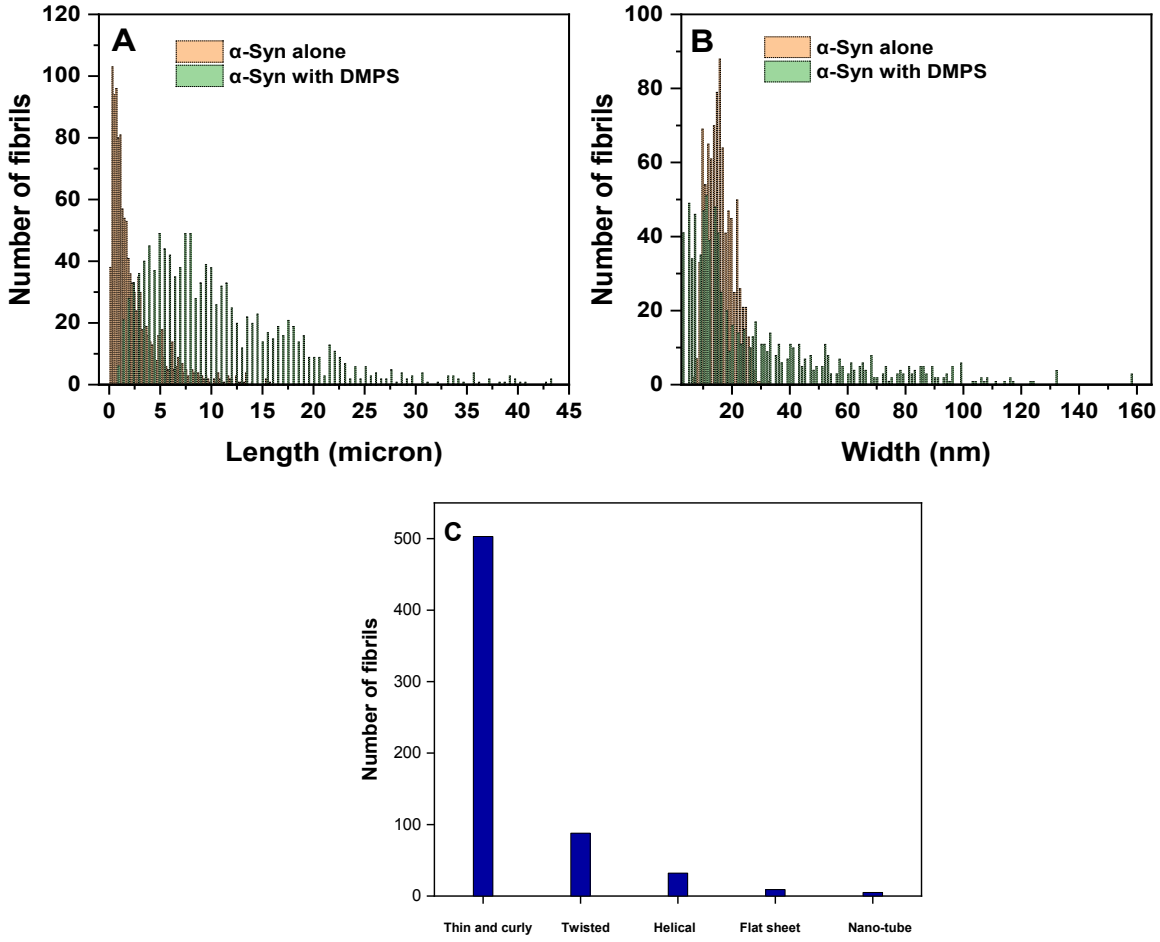

Figure 6. Quantitative analysis of TEM images of fibrils. (A) Distribution of contour length of α-syn fibrils. (N = 900) **(B)** Distribution of width of α-syn fibril (N = 1200). These results show that in the presence of DMPS the contour length and width of the fibrils has much higher distribution than in its absence. **(C)** Relative abundance of polymorphs (N = 637). This data imply that thin and curly amyloid fibrils have highest abundance followed by twisted, helical, flat sheet and nano-tubes, respectively.

Helical pitch and width are important parameters often used to identify the polymorphs of amyloid fibrils[23]. A helical pitch is defined as the distance along the fibril length that it takes for the helix to complete one 360° turn. **Fig. 7** shows the relationship between helical pitch and fibril width for multiple helical fibrils. We found that the helical pitch ranged from 245 to 3373 nm and widths spanned from 15 to 157 nm. Moreover, we found that the helical pitch is linearly correlated with the width of the fibrils measured. Previous work on other polymorphic amyloid fibril systems demonstrated a similar relationship[22,68]. In those works, they found a very strong linear relationship with little variation from the linear model whereas we observe more variation. One interpretation of this finding is that this may imply there are different structural

arrangements or interactions occurring between the constituent protofibrils which gives rise to the structural variations we see. However, more work needs to be done in order to confirm this hypothesis.

The large widths observed for the twisted and helical ribbon polymorphs suggest that they are composed of a number of protofilaments. This observation is consistent with models that consider hierarchical assembly of protofilaments into larger amyloid fibril polymorphs[15,68]. Indeed, we observe several helical and twisted ribbons that appear to split along the length of the fibril (**Fig. 8 and S3**). Moreover, we see that this splitting can happen at multiple locations along the length of single fibril. The individual strands of these "frayed" fibrils have a larger width than that observed for protofilaments (3 nm). This implies that fibrils consisting of many protofibrils may further assemble to produce giant fibrils in a hierarchical assembly. It is important to note that we were unable to determine the length and position of individual fibrils in hierarchically assembled fibrils. This means that we cannot rule out the possibility that mature fibrils may join at different positions on laterally assembling fibrils to form such long fibrils. However, our study does demonstrate that α-syn fibrils formed in the presence of lipid vesicles are much longer than those formed in the absence of lipid vesicles.

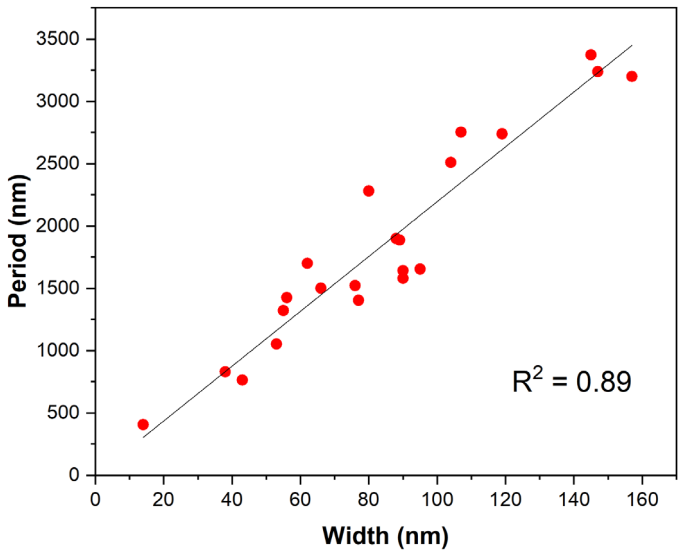

Figure 7. **Helical pitch of twisted ribbons plotted against width of the fibrils**. This result shows a linear relation between fibril width and helical pitch of α-syn amyloid fibrils formed in the presence of DMPS vesicles.

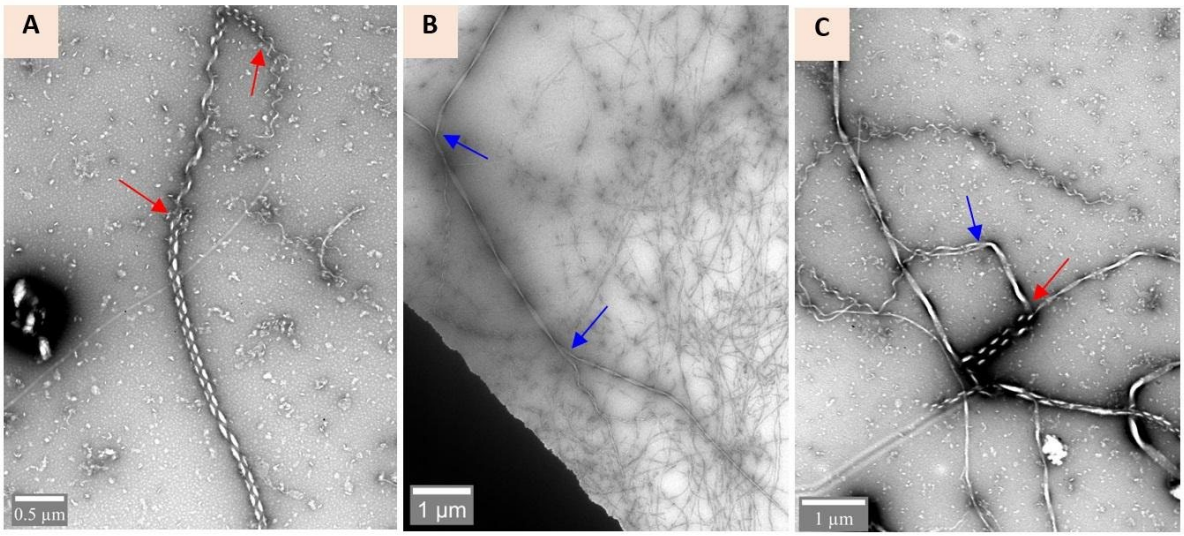

Figure 8. TEM imaging of fibril splitting: Fibrils show splitting along their length as shown in **A-C**. Splitting was observed for both helical (marked with red arrow) and twisted (marked with blue arrow) fibrils. This result shows that observed giant fibrils are composed of mature fibrils.

Fibril formed in the presence of DMPS vesicles co-localize with lipid molecules

Previous *in vitro* studies have shown that co-assembly can occur between lipid molecules and α-syn during amyloid fibril formation[71,72], and in a recent study it has been shown that Lewy bodies, the hallmark of Parkinson's disease, consist of highly crowded mixtures of organellar and membranous features that contain inclusions of α-syn[73]. Interestingly, in another study, incubation of α-syn on a supported bilayer of phospholipid membrane resulted in the aggregation of α-syn accompanied by lipid extraction from the membrane, causing membrane disruption and clustering of lipid molecules around growing α-syn aggregates[74]. To see whether α-syn fibrils can incorporate lipid, we employed TIRF microscopy to image individual α-syn aggregates (SAVE imaging)[74]. For these experiments, we utilised a previously published approach in which the DMPS liposomes are mixed with biotinylated lipid[75]. These biotinylated liposomes were added to our α-syn samples and allowed to undergo fibrilization. Samples were collected and incubated with Alexa Fluor 647 labeled streptavidin (1 nM) and 5 uM ThT to allow for simultaneous imaging and localization of lipids and fibrils, respectively. We found a high degree of co-localization of the lipids and fibrils **(Fig 9)**. In contrast, when fibrils were prepared without biotinylated lipids, no co-localization was observed (**Figs. S5**). The association quotient, Q[76–78] (see single-molecule data analysis in Methods), is a measure of the

level of coincidence of the fibrils and lipids. For these samples, $Q = 0.43 \pm 0.17$ (mean ± S.D., $n = 27$ images), indicating that 43% of the fibrils identified contained biotinylated lipid. For the control in which biotinylated lipid was not included, $Q = -0.02 \pm 0.04$ (mean ± S.D., $n = 5$ images).

Taken together, these imaging techniques demonstrate that in the presence of DMPS lipid vesicles, the growing fibrils can directly incorporate lipid molecules. Further study of these highly polymorphic α-syn amyloid fibril variants can better illuminate the processes that govern lipid-induced conversion of α-syn into potentially pathological forms.

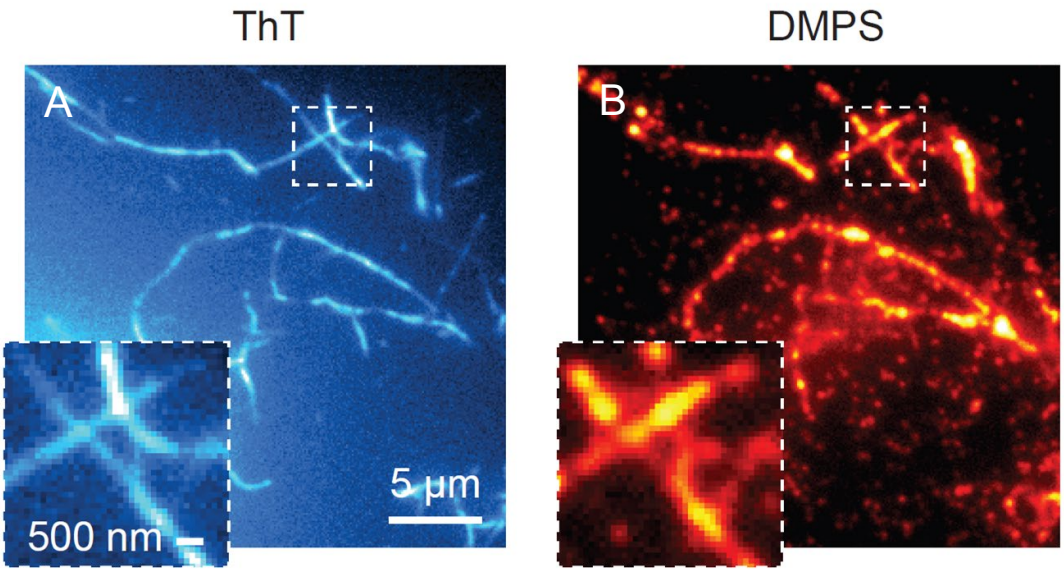

Figure 9. α-Syn amyloid fibrils association with lipid observed by TIRFM imaging. 0.5 µM α-syn amyloid fibrils and in the presence of 4 mM DMPS vesicles (containing 2 mol % of biotinylated lipid) in the presence of 1 nM streptavidin-AF647 and 5 mM ThT **(A)** Images were recorded for 50 frames from the red channel (AF647 emission) with 641 nm illumination, followed by **(B)** green channel (ThT emission) with 405 nm illumination.

DISCUSSION

With a growing number of studies, it is becoming increasingly clear that heterogenous nucleation plays an important role in amyloid formation in different amyloid forming proteins. Most importantly, many studies have shown interactions between lipid bilayers and amyloid forming proteins is a common triggering event in the formation of amyloid fibrils and other cytotoxic species[79–81]. Current evidence suggests that lipid membranes provide a platform where the binding of amyloidogenic protein increases the local concentration of bound protein

molecules and thus facilitates the formation of toxic aggregates. In the work reported here, we have explored the effect of physiological relevant lipid DMPS on α-syn fibrillization.

Analysis of ThT fluorescence data showed that with an increase in the L/P ratio, lag-time was significantly decreased (**Fig. 2**). Interestingly, the kinetic curves of samples incubated in the presence of DMPS vesicles show biphasic fluorescence **(Fig S1).** Similar kinetic profiles have been observed in a study in which α-syn was incubated with brain tissue from PD patient's frontal and temporal cortex samples[82]. Similarly, another study that incubated α-syn with lipid vesicles at higher temperature also reported a comparable biphasic increase in ThT fluorescence intensity[83]. The reason for these biphasic increase in the ThT fluorescence intensity is not clear.

TEM imaging of the samples revealed the presence of a large spectrum of amyloid fibril structures when α-syn was aggregated in the co-presence of DMPS vesicles. At an L/P ratio of 8, we identified multiple structures such as thin and curly fibrils, twisted and helical ribbons, nanotubes and flat sheets (**Fig. 3D-L and 4**). Although all of these structures have been reported before for amyloid forming proteins and short peptides, no study has described the presence of so many variants under identical environmental conditions. We further investigated the impact of L/P ratios ranging from 1 to 4 on the morphology of the fibrils. We found that these ratios strongly affect the morphology of α-syn fibrils (**Fig. 5**). We speculate that higher L/P ratios effectively cover the fibrils surface and thereby promote their lateral association by hydrophobic interaction. However, we acknowledge that further studies are required to confirm our hypothesis.

When we carried out the reaction in the absence of DMPS, we observed either small oligomeric aggregates or straight fibrils with rod-like morphologies (**Fig. 3A- 3C**). Quantitative analysis of these fibrils showed they possess a wide spectrum of lengths and widths as compared to fibrils in the absence of DMPS (**Fig. 6A-B**). Further analysis of the width-to-period relation of twisted ribbons showed a linear relationship, which suggest these fibrils have a different number of constituent protofilaments (**Fig. 7**). These results clearly show that the presence of DMPS vesicles not only modulates the kinetics of fibril formation of α-syn but importantly, its interaction leads to the formation of polymorphic fibril forms. Polymorphic forms of α-syn are known to be present under *in vivo* conditions and they have been linked to different pathological conditions[24,27,84–86], however, factors responsible for formation of these

polymorphs under *in vivo* conditions are not known. The findings of our present study highlight the possible role lipids play in the formation of α-syn polymorphs under *in vivo* conditions.

Previous reports of lipid molecule clustering on growing α-syn fibrils[74] prompted us to investigate if lipid molecules are being directly incorporated into amyloid fibrils. Experiments carried out with TIRF microscopy shows a high-level of co-localization of lipid and amyloid fibrils (**Fig. 9**). Thus, we confirmed that lipids can be incorporated into the structure of amyloid fibrils during their growth process. Notably, in a recent cryo-EM study by Benedikt *et al.*[54], six polymorphs of α-syn were observed in the presence of POPA/POC lipid vesicles, all of which were coated with lipid molecules. Moreover, in polymorph L1B, which consists of two identical protofilaments, a wide cavity in the inter-protofilament interface was observed. These cavities were found to contain lipid molecules, and both the head-group and acyl-chains of anionic lipid made specific contacts with amino acid residues in the protofilaments. In another polymorph L2A, which consists of three protofilaments that are 20 Å apart and show no direct protein-protein contact, an ordered interaction network of negatively charged head-group and acyl-chain lipids was observed. Although Benedikt *et al*. elegantly demonstrated that lipid molecules were incorporated into fibrils, which stabilised alternative quaternary fold, it should be noted that they used phospholipid with a phosphatidic acid (PA) head-group, whereas a phosphatidylserine (PS) head-group used in our study. PS contains a serine molecule attached to a phosphate group, whereas PA only has a phosphate group. Additionally, the acyl chain length and saturation state differ between DMPS and DOPA, with 14:0-14:0 and 18:1,18:1 for DMPS and DOPA, respectively. Therefore, the fibrils formed in the presence of these two molecules will be different. Furthermore, lipid profiling shows the content of PS is about 40 times higher than PA in mouse brain[87], and there is a significant increase in PS content in the brain of PD patients and animal models[88,89].These findings suggest that PS may play a crucial role in the pathogenesis of PD, highlighting the need to understand its importance in α-syn aggregation.

In summary, we have shown that under *in vitro* conditions, lipid-protein interactions play an important role in the formation of polymorphs of α-syn amyloid fibrils. Further study is needed to understand the mechanism of the lipid-induced conversion of α-syn into its polymorphic forms. The knowledge obtained from such a study is also expected to provide crucial information on the widely observed lipid-induced conversion of amyloid forming proteins into their toxic forms.

METHODS

Reagents

1,2-dimyristoyl-sn-glycero-3-phospho-L-serine (DMPS) lyophilized powder and 1,2-distearoyl-sn-glycero-3-phosphoethanol-amine-N-[amino(polyethyleneglycol0)] (DSPE-PEG) were purchased from Avanti Polar Lipid, Inc. Streptavidin, Alexa Fluor 647 conjugate was purchased from ThermoFisher Scientific. Tris base, ethylenediaminetetraacetic acid (EDTA), Thioflavin T, Chloroform, Methanol, and Hydrochloric acid (HCl) and other chemicals were purchased from Sigma Aldrich.

Protein purification. Recombinant WT α-syn was expressed in *Escherichia Coli* and purified as described previously[90].

Liposome preparation

About 1 mg DMPS were obtained in a glass test-tube and dissolved in chloroform:methanol (3:1 v/v) solvent. Thin layer of lipid was obtained by constant rotating of test-tube, while gentle stream of nitrogen gas was used to evaporate the solvent. To remove the any trace amount of solvent, test-tube was placed in the vacuum for minimum of 4h. Liposome biotinylation was achieved by adding 2 mol % of biotinylated lipid (DSPE-PEG Biotin, Avanti) to DMPS lipid. The thin lipid layer was then hydrated with appropriate amount of 25 mM Tris buffer, pH 7.4 to make a stock concentration of 2 mM and vortexed for 2 mins to dissolve the lipid layer in the buffer. Sample was frozen and thawed for 4 cycle on dry ice and water-bath at 40 °C. Small unilamellar vesicles (SUVs) were prepared by sonication (VWR ultrasonic cleaner) for 30 minutes.

Dynamic light scattering (DLS)

Size distribution of lipid vesicles was determined by an ALV/CGS-3 platform-based goniometer system (ALV-GmbH). This instrument was equipped with a 22 mW HeNe laser with a wavelength of 633 nm, and backscattered light was detected at an angle of 90^{o} at room temperature. DMPS stock solutions were diluted to 60 μM in filtered 25 mM Tris buffer (pH

7.4), transferred into glass test tube, and placed in the measurement cell. Three measurements were performed for the sample for 300 seconds at room temperature and average values were used for analysing the data. The analysis showed that the data consisted of two peaks, a small peak centered at a diameter of 17 nm and a large peak centered at a diameter of 109 nm. This is similar to the findings of a previous report[35] **(Fig. S6)**.

Aggregation assay

ThT fluorescence time-course measurements were performed in 96-well microliter plates using Fluostar Omega microplate reader (BMG Labtech) with excitation and emission wavelengths set to 450 nm and 485 nm. 50 μM WT α-syn samples were prepared in the absence and presence of 25 μM, 50 μM, 100 μM, 200 μM and 400 μM of DMPS vesicles with 25 μM ThT in 25 mM Tris buffer (pH 7.4). Each sample-well contained 100 μL of the reaction mixture and spontaneous aggregation was induced by incubation at 30 ^{o}C without shaking.

Transmission electron microscopy

At the end of aggregation assay, aggregated sample was diluted to 1 mM concentration. An aliquot (7 mL) of diluted sample was placed onto carbon support film 300 Mesh 3 mm copper grids (TAAB) for 3 min and blot dried. The TEM grids were subsequently stained using 7 mL of 1 % uranyl acetate for 2 min followed by blot drying. Samples were imaged on a Thermo Fisher Scientific Tecnai F20 electron microscope (200 kV, field emission gun) equipped with an 8k x 8k CMOS camera (TVIPS F816).

CD Spectroscopy

A Jasco J-810 spectrometer was used for CD measurements. Samples containing 10 μM WT α-syn in presence of different amount of DMPS (0, 10, 20, 30, 40, 50, 60, 70, 80, 90, 100, 110, 120, 130, 140, 150, 160, 170, 200, 250 and 300 μM) were prepared in 25 mM phosphate buffer (pH 7.4). Experiments were performed at 30 °C using a quartz cuvette with 1 mm path length at a scan rate 20 nm min^{-1} with a data pitch of 0.1 nm and a digital integration time of 1s. A total five scan were accumulated and averaged for a final data.

Slide preparation for single-molecule analysis

Glass coverslips (22 × 22 mm, VWR international, USA) were cleaned using an argon plasma cleaner (Zepto, Diener, Germany) for 40 minutes to remove any fluorescent residue. Frame-seal slide chambers (9 x 9 cm^2, Bio-Rad, Hercules, USA) were affixed to the glass, 50 µl of poly-L-lysine (70-150k molecular weight, Sigma-Aldrich) was added and incubated at room temperature for at least 15 minutes. The coverslips were washed twice with 25 mM filtered buffer (25 mM Tris, pH 7.4) immediate before adding the sample for imaging.

Total internal reflection fluorescence microscopy

Single-molecule imaging was performed using a custom-built single-molecule TIRF microscope, which restricts the illumination to within ~200 nm of the sample slide. The fluorophores were excited at either 405 nm (ThT), or 638 nm (AF647). Collimated laser light at wavelengths of 405 nm (Cobolt MLD Series 405- 250 Diode Laser System, Cobolt AB, Solna, Sweden), and 638 nm (Cobolt MLD Series 638-140 Diode Laser System, Cobolt AB, Solna, Sweden) were aligned and directed parallel to the optical axis at the edge of a 1.49 NA TIRF objective (CFI Apochromat TIRF 60XC Oil, Nikon, Japan), mounted on an inverted Nikon TI2 microscope (Nikon, Japan). The microscope was fitted with a perfect focus system to autocorrect the z-stage drift during imaging. Fluorescence collected by the same objective was separated from the returning TIR beam by a dichroic mirror (Di01-R405/488/ 561/635 (Semrock, Rochester, NY, USA), and was passed through appropriate filters (405 nm: BLP01-488R-25 (Semrock, Rochester, NY, USA), 638 nm: FF01-692/40−25 (Semrock, Rochester, NY, USA). The fluorescence was then passed through a 2.5× beam expander and recorded on an EMCCD camera (Delta Evolve 512, Photometrics, Tucson, AZ, USA) operating in frame transfer mode (EMGain = 11.5 e−/ ADU and 250 ADU/photon). Each pixel was 103 nm in length. Images were recorded over 10 frames with an exposure time of 50 ms with 638 nm (~50 W cm^{-2}) illumination, followed by 405 nm excitation (~100 W cm^{-2}). The microscope was automated using the open-source microscopy platform Micromanager.

Sample collected from a 96 well-plate after completion of aggregation reaction was diluted 100 × and incubated for 10 minutes in presence of 1 nM Straptavidin-AF647 (ThermoFisher Scientific). It was then centrifuged at 14k rpm for 10 minutes and the pellet was redissolved in 5 µM ThT and placed on glass coverslip for imaging.

Single-molecule data analysis

The data were analysed using a custom-written code in Igor Pro (Wavemetrics). Each tiff image stack was first averaged over the 10 frames in each channel, before having the background subtracted. A manual threshold value of 1000 ADU (ThT channel) was used to distinguish fibrils from background. A clustering algorithm (Density-based spatial clustering of applications with noise)[91] was used to identify individual fibrils. For each fibril, the corresponding fluorescence was analysed in the AF647 channel for each pixel, and a positive coincidence was defined if at least one of these had a value greater than an applied threshold of 1500 ADU in the AF647 channel. To account for chance coincidence (i.e. due to the fibrils and AF647-tagged liposomes being in close proximity), the same analysis was performed with the AF647 images being rotated 90° and translated 100 pixels. For each image set, the association quotient, Q[76–78], which is a measure of coincidence, was calculated according to Equation 1.

Equation 1 $$Q = \frac{C-E}{A-E}$$

Where C is the number of coincident events, E the number of chance events, and A the total number of fibrils detected.

Acknowledgments

This work was supported by The Royal Society UK, and Science and Engineering Research Board (SERB), India. M.H.H. acknowledges funding from the UK Dementia Research Institute and UCB to build the total internal reflection fluorescence microscope (https://www.ucb.com).

References

1. Graumann PL (2004) Cytoskeletal elements in bacteria. Curr. Opin. Microbiol. 7:565–571.
2. Kueh HY, Mitchison TJ (2009) Structural Plasticity in Actin and Tubulin Polymer Dynamics. Science. 325:960–963.
3. Ryan EA, Mockros LF, Weisel JW, Lorand L (1999) Structural Origins of Clot Rheology. Biophys. J. 77:2813–2826.
4. Buehler MJ (2006) Nature designs tough collagen: Explaining the nanostructure of collagen fibrils. Proc. Natl. Acad. Sci. U. S. A. 103:12285–12290.
5. Römer L, Scheibel T (2008) The elaborate structure of spider silk: structure and function

of a natural high performance fiber. Prion 2:154–161.
6. Chiti F, Dobson CM (2006) Protein Misfolding, Functional Amyloid, and Human Disease. Annu. Rev. Biochem. 75:333–366.
7. Knowles TPJ, Mezzenga R (2016) Amyloid Fibrils as Building Blocks for Natural and Artificial Functional Materials. Adv. Mater. 28:6546–6561.
8. Knowles TPJ, Buehler MJ (2011) Nanomechanics of functional and pathological amyloid materials. Nat. Nanotechnol. 6:469–479.
9. Khurana R, Ionescu-Zanetti C, Ionescu-Zanetti et al. (2003) A general model for amyloid fibril assembly based on morphological studies using atomic force microscopy. Biophys. J. 85:1135–44.
10. Knowles TPJ, Vendruscolo M, Dobson CM (2014) The amyloid state and its association with protein misfolding diseases. Nat. Rev. Mol. Cell Biol. 15:384–396.
11. Eisenberg D, Jucker M (2012) The amyloid state of proteins in human diseases. Cell 148:1188–1203.
12. Nelson R, Sawaya MR, Balbirnie M, Madsen A, Riekel C, Grothe R, Eisenberg D (2005) Structure of the cross-β spine of amyloid-like fibrils. Nature 435:773–778.
13. Li B, Ge P, Murray KA, Sheth P, Zhang M, Nair G, Sawaya MR, Shin WS, Boyer DR, Ye S, et al. (2018) Cryo-EM of full-length α-synuclein reveals fibril polymorphs with a common structural kernel. Nat. Commun. 9:1–10.
14. Elizabeth L. Guenther, Peng Ge, Hamilton Trinh, Michael. Sawaya, Duilio Cascio, David R. Boyer, Tamir Gonen, Z. Hong Zhou and DSE (2018) Atomic-level evidence for packing and positional amyloid polymorphism by segment from TDP-43 RRM2. Nat Struct Mol Biol. 25:311–319.
15. Fitzpatricka AWP, Debelouchinac GT, Bayroc et al. (2013) Atomic structure and hierarchical assembly of a cross-β amyloid fibril. Proc Natl Acad Sci USA 5590:5468–5473.
16. Anthony W.P. et al. (2017) Cryo-EM structures of Tau filaments from Alzheimer's disease brain. Nature 547:185–190.
17. Guerrero-Ferreira R, Taylor NMI, Mona D, Ringler P, Lauer ME, Riek R, Britschgi M, Stahlberg H (2018) Cryo-EM structure of alpha-synuclein fibrils. Elife 7:1–18.
18. Li Y, Zhao C, Luo F, Liu Z, Gui X, Luo Z, Zhang X, Li D, Liu C, Li X (2018) Amyloid fibril structure of α-synuclein determined by cryo-electron microscopy. Cell Res. 28:897–903.
19. Chien P, Weissman JS, DePace AH (2004) Emerging Principles of Conformation-Based Prion Inheritance. Annu. Rev. Biochem. 73:617–656.

20. Qiang W, Yau WM, Lu JX, Collinge J, Tycko R (2017) Structural variation in amyloid-β fibrils from Alzheimer's disease clinical subtypes. Nature 541:217–221.
21. Adamcik J, Mezzenga R (2018) Amyloid Polymorphism in the Protein Folding and Aggregation Energy Landscape. Angew. Chemie - Int. Ed. 57:8370–8382.
22. Lara C, Adamcik J, Jordens S, Mezzenga R (2011) General self-assembly mechanism converting hydrolyzed globular proteins into giant multistranded amyloid ribbons. Biomacromolecules 12:1868–1875.
23. Marcus Fändrich et al. (2018) Amyloid fibril polymorphism - a challenge for molecular imaging and therapy. J Intern Med. 283:218–237.
24. Lau A, So RWL, Lau HHC, Sang JC, Ruiz-Riquelme A, Fleck SC, Stuart E, Menon S, Visanji NP, Meisl G, et al. (2020) α-Synuclein strains target distinct brain regions and cell types. Nat. Neurosci. 23:21–31.
25. Lu JX, Qiang W, Yau WM, Schwieters CD, Meredith SC, Tycko R (2013) Molecular structure of β-amyloid fibrils in alzheimer's disease brain tissue. Cell 154:1257–68.
26. Aneta T. Petkova, Richard D. Leapman, Zhihong Guo, Wai-Ming Yau, Mark P. Mattson RT (2005) Self-Propagating, Molecular-Level Polymorphism in Alzheimer's □-Amyloid Fibrils. Science. 307:262–265.
27. Peelaerts W, Baekelandt V (2016) α-Synuclein strains and the variable pathologies of synucleinopathies. J. Neurochem. 139:256–274.
28. Goedert M, Jakes R, Spillantini MG (2017) The Synucleinopathies: Twenty Years on. J. Parkinsons. Dis. 7:S53–S71.
29. Peelaerts W, Bousset L, Van Der Perren A et al. (2015) α-Synuclein strains cause distinct synucleinopathies after local and systemic administration. Nature 522:340–344.
30. Galvagnion C (2017) The Role of Lipids Interacting with α-Synuclein in the Pathogenesis of Parkinson's Disease. J. Parkinsons. Dis. 7:433–450.
31. Bendor JT, Logan TP, Edwards RH (2013) The function of α-synuclein. Neuron 79:1044–1066.
32. Beatman EL, Massey A, Shives KD, Burrack KS, Chamanian M, Morrison TE (2016) Alpha-Synuclein Expression Restricts RNA Viral Infections in the Brain. J. Virol. 90:2767–2782.
33. de Diego I, Peleg S, Fuchs B (2019) The role of lipids in aging-related metabolic changes. Chem. Phys. Lipids 222:59–69.
34. Shulman JM, De Jager PL, Feany MB (2011) Parkinson's disease: Genetics and pathogenesis. Annu. Rev. Pathol. Mech. Dis. 6:193–222.

35. Galvagnion C, Buell AK, Meisl G, Michaels TCT, Vendruscolo M, Knowles TPJ, Dobson CM (2015) Lipid vesicles trigger α-synuclein aggregation by stimulating primary nucleation. Nat. Chem. Biol. 11:229–234.

36. Ross BM, Mamalias N, Moszczynska A, Rajput AH, Kish SJ (2001) Elevated activity of phospholipid biosynthetic enzymes in substantia nigra of patients with Parkinson's disease. Neuroscience 102:899–904.

37. Horrocks MH, Lee SF, Gandhi S, Magdalinou NK, Chen SW, Devine MJ, Tosatto L, Kjaergaard M, Beckwith JS, Zetterberg H, et al. (2016) Single-Molecule Imaging of Individual Amyloid Protein Aggregates in Human Biofluids. ACS Chem. Neurosci. 7:399–406.

38. Fusco G, De Simone A, Gopinath T, Vostrikov V, Vendruscolo M, Dobson CM, Veglia G (2014) Direct observation of the three regions in α-synuclein that determine its membrane-bound behaviour. Nat. Commun. 5:1–17.

39. Ferreon ACM, Deniz AA (2007) α-Synuclein multistate folding thermodynamics: Implications for protein misfolding and aggregation. Biochemistry 46:4499–4509.

40. Anderson VL, Ramlall TF, Rospigliosi CC, Webb WW, Eliezer D (2010) Identification of a helical intermediate in trifluoroethanol-induced alpha-synuclein aggregation. Proc. Natl. Acad. Sci. 107:18850–18855.

41. Munishkina LA, Phelan C, Uversky VN, Fink AL (2003) Conformational behavior and aggregation of α-synuclein in organic solvents: Modeling the effects of membranes. Biochemistry 42:2720–2730.

42. Kuznetsova IM, Turoverov KK, Uversky VN (2004) Use of the phase diagram method to analyze the protein unfolding-refolding reactions: Fishing out the "invisible" intermediates. J. Proteome Res. 3:485–494.

43. Ferreon ACM, Gambin Y, Lemke EA, Deniz AA (2009) Interplay of α-synuclein binding and conformational switching probed by single-molecule fluorescence. Proc. Natl. Acad. Sci. U. S. A. 106:5645–5650.

44. Georgieva ER, Ramlall TF, Borbat PP, Freed JH, Eliezer D (2008) Membrane-bound α-synuclein forms an extended helix: Long-distance pulsed ESR measurements using vesicles, bicelles, and rodlike micelles. J. Am. Chem. Soc. 130:12856–12857.

45. Viennet T, Wördehoff MM, Uluca B, Poojari C, Shaykhalishahi H, Willbold D, Strodel B, Heise H, Buell AK, Hoyer W, et al. (2018) Structural insights from lipid-bilayer nanodiscs link α-Synuclein membrane-binding modes to amyloid fibril formation. Commun. Biol. 1:44.

46. Rao JN, Jao CC, Hegde BG, Langen R, Ulmer TS (2010) A combinatorial NMR and EPR

approach for evaluating the structural ensemble of partially folded proteins. J. Am. Chem. Soc. 132:8657–8668.
47. Bodner CR, Dobson CM, Bax A (2009) Multiple Tight Phospholipid-Binding Modes of α-Synuclein Revealed by Solution NMR Spectroscopy. J. Mol. Biol. 390:775–790.
48. Gursky O, Atkinson D (1996) High- and low-temperature unfolding of human high-density apolipoprotein A-2. Protein Sci. 5:1874–1882.
49. Eugène S, Xue WF, Robert P, Doumic M (2016) Insights into the variability of nucleated amyloid polymerization by a minimalistic model of stochastic protein assembly. J Chem Phys 144:175101.
50. Gaspar R, Pallbo J, Weininger U, Linse S, Sparr E (2018) Ganglioside lipids accelerate α-synuclein amyloid formation. Biochim. Biophys. Acta - Proteins Proteomics 1866:1062–1072.
51. Wei G, Su Z, Reynolds NP, Arosio P, Hamley IW, Gazit E, Mezzenga R (2017) Self-assembling peptide and protein amyloids: From structure to tailored function in nanotechnology. Chem. Soc. Rev. 46:4661–4708.
52. Adamcik J, Sánchez-Ferrer A, Ait-Bouziad N, Reynolds NP, Lashuel HA, Mezzenga R (2016) Microtubule-Binding R3 Fragment from Tau Self-Assembles into Giant Multistranded Amyloid Ribbons. Angew. Chemie - Int. Ed. 55:618–622.
53. Zhu M, Fink AL (2003) Lipid binding inhibits α-synuclein fibril formation. J. Biol. Chem. 278:16873–16877.
54. Benedikt et al. (2022) The 3D structure of lipidic fibrils of α -synuclein. Nat. Commun. 13(1):6810.
55. Galvagnion C, Brown JWP, Ouberai MM, Flagmeier P, Vendruscolo M, Buell AK, Sparr E, Dobson CM (2016) Chemical properties of lipids strongly affect the kinetics of the membrane-induced aggregation of α-synuclein. Proc. Natl. Acad. Sci. 113:7065–7070.
56. Guerrero-Ferreira R, Taylor NMI, Arteni AA, Kumari P, Mona D, Ringler P, Britschgi M, Lauer ME, Makky A, Verasdock J, et al. (2019) Two new polymorphic structures of human full-length alpha-synuclein fibrils solved by cryo-electron microscopy. Elife 8:1–24.
57. Periole X, Huber T, Bonito-Oliva A, Aberg KC, Van Der Wel PCA, Sakmar TP, Marrink SJ (2018) Energetics Underlying Twist Polymorphisms in Amyloid Fibrils. J. Phys. Chem. B 122:1081–1091.
58. Seetaloo N, Zacharopoulou M, Stephens AD, Schierle GSK, Phillips JJ (2022) Local structural dynamics of alpha-synuclein correlate with aggregation in different physiological conditions. bioRxiv:2022.02.11.480045.

59. Lu K, Jacob J, Thiyagarajan P, Conticello VP, Lynn DG (2003) Exploiting amyloid fibril lamination for nanotube self-assembly. J. Am. Chem. Soc. 125:6391–6393.
60. Aggeli A, Nyrkova IA, Bell M, Harding R, Carrick L, McLeish TCB, Semenov AN, Boden N (2001) Hierarchical self-assembly of chiral rod-like molecules as a model for peptide -sheet tapes, ribbons, fibrils, and fibers. Proc. Natl. Acad. Sci. 98:11857–11862.
61. Lamm MS, Rajagopal K, Schneider JP, Pochan DJ (2005) Laminated morphology of nontwisting β-sheet fibrils constructed via peptide self-assembly. J. Am. Chem. Soc. 127:16692–16700.
62. Pashuck ET, Stupp SI (2010) Direct observation of morphological tranformation from twisted ribbons into helical ribbons. J. Am. Chem. Soc. 132:8819–8821.
63. Zhang S, Andreasen M, Nielsen JT, Liu L, Nielsen EH, Song J, Ji G, Sun F, Skrydstrup T, Besenbacher F, et al. (2013) Coexistence of ribbon and helical fibrils originating from hIAPP 20-29 revealed by quantitative nanomechanical atomic force microscopy. Proc. Natl. Acad. Sci. U. S. A. 110:2798–2803.
64. Serpell LC, Berriman J, Jakes R, Goedert M, Crowther RA (2000) Fiber diffraction of synthetic alpha -synuclein filaments shows amyloid-like cross-beta conformation. Proc. Natl. Acad. Sci. 97:4897–4902.
65. Paravastu AK, Leapman RD, Yau WM, Tycko R (2008) Molecular structural basis for polymorphism in Alzheimer's β-amyloid fibrils. Proc. Natl. Acad. Sci. U. S. A. 105:18349–18354.
66. Marcus D. Tuttle et al. (2016) Solid-State NMR Structure of a Pathogenic Fibril of Full-Length Human α-Synuclein. Nat Struct Mol Biol. 23:409–415.
67. Jose A. Rodriguez et al. (2015) Structure of the toxic core of α-synuclein from invisible crystals. Nature 525:486–490.
68. Adamcik J, Jung J-M, Flakowski J, De Los Rios P, Dietler G, Mezzenga R (2010) Understanding amyloid aggregation by statistical analysis of atomic force microscopy images. Nat. Nanotechnol. 5:423–428.
69. Fecchio C, Palazzi L, Polverino de Laureto P (2018) α-Synuclein and polyunsaturated fatty acids: Molecular basis of the interaction and implication in neurodegeneration. Molecules 23(7),1531.
70. Usov I, Adamcik J, Mezzenga R (2013) Polymorphism complexity and handedness inversion in serum albumin amyloid fibrils. ACS Nano 7:10465–10474.
71. Hellstrand E, Nowacka A, Topgaard D, Linse S, Sparr E (2013) Membrane Lipid Co-Aggregation with α-Synuclein Fibrils. PLoS One 8(10), e77.

72. Galvagnion C, Topgaard D, Makasewicz K, Buell AK, Linse S, Sparr E, Dobson CM (2019) Lipid Dynamics and Phase Transition within α-Synuclein Amyloid Fibrils. J. Phys. Chem. Lett. 10:7872–7877.
73. Shahmoradian SH et al. (2019) Lewy pathology in Parkinson's disease consists of crowded organelles and lipid membranes. Nat. Neurosci. 22:1099–1109.
74. Reynolds NP, Soragni A, Rabe M, Verdes D, Liverani E, Handschin S, Riek R, Seeger S (2011) Mechanism of membrane interaction and disruption by α-synuclein. J. Am. Chem. Soc. 133:19366–19375.
75. Choi ML, Chappard A, Singh BP et al. (2022) Pathological structural conversion of α-synuclein at the mitochondria induces neuronal toxicity. Nat. Neurosci. 25:1134–1148.
76. Raynes JK, Day L, Crepin P, Horrocks MH, Carver JA (2017) Coaggregation of κ-Casein and β-Lactoglobulin Produces Morphologically Distinct Amyloid Fibrils. Small 13:1–11.
77. Benson S et al. (2019) SCOTfluors: Small, Conjugatable, Orthogonal, and Tunable Fluorophores for In Vivo Imaging of Cell Metabolism. Angew. Chemie - Int. Ed. 58:6911–6915.
78. Janeczek AA, Scarpa E, Horrocks MH, Tare RS, Rowland CA, Jenner D, Newman TA, Oreffo ROC, Lee SF, Evans ND (2017) PEGylated liposomes associate with Wnt3A protein and expand putative stem cells in human bone marrow populations. Nanomedicine 12:845–863.
79. Gal N, Morag A, Kolusheva S, Winter R, Landau M, Jelinek R (2013) Lipid bilayers significantly modulate cross-fibrillation of two distinct amyloidogenic peptides. J. Am. Chem. Soc. 135:13582–13589.
80. Hebda JA, Miranker AD (2009) The Interplay of Catalysis and Toxicity by Amyloid Intermediates on Lipid Bilayers: Insights from Type II Diabetes. Annu. Rev. Biophys. 38:125–152.
81. Khondker A, Alsop RJ, Rheinstädter MC (2017) Membrane-accelerated Amyloid-β aggregation and formation of cross-β sheets. Membranes (Basel). 7(3), 49.
82. Ghanem SS, Majbour NK, Vaikath NN, Ardah MT, Erskine D, Jensen NM, Fayyad M, Sudhakaran IP, Vasili E, Melachroinou K, et al. (2022) α-Synuclein phosphorylation at serine 129 occurs after initial protein deposition and inhibits seeded fibril formation and toxicity. Proc. Natl. Acad. Sci. U. S. A. 119.
83. Brown JWP, Meisl G, Knowles TPJ, Buell AK, Dobson CM, Galvagnion C (2018) Kinetic barriers to α-synuclein protofilament formation and conversion into mature fibrils. Chem. Commun. 54:7854–7857.

84. Wiltzius JJW, Landau M, Nelson R, Sawaya MR, Apostol MI, Goldschmidt L, Soriaga AB, Cascio D, Rajashankar K, Eisenberg D (2009) Molecular mechanisms for protein-encoded inheritance. Nat. Struct. Mol. Biol. 16:973–978.
85. Shahnawaz M, Mukherjee A, Pritzkow S, Mendez N, Rabadia P, Liu X, Hu B, Schmeichel A, Singer W, Wu G, et al. (2020) Discriminating α-synuclein strains in Parkinson's disease and multiple system atrophy. Nature 578:273–277.
86. Annamalai K, Gührs KH, Koehler R, Schmidt M, Michel H, Loos C, Gaffney PM, Sigurdson CJ, Hegenbart U, Schönland S, et al. (2016) Polymorphism of Amyloid Fibrils in Vivo. Angew. Chemie - Int. Ed. 55:4822–4825.
87. Kilaru A, Isaac G, Tamura P, Baxter D, Duncan SR, Venables BJ, Welti R, Koulen P, Chapman KD (2010) Lipid Profiling Reveals Tissue-Specific Differences for Ethanolamide Lipids in Mice Lacking Fatty Acid Amide Hydrolase. Lipids 45:863–875.
88. Fabelo N, Martín V, Santpere G, Marín R, Torrent L, Ferrer I, Díaz M (2011) Severe alterations in lipid composition of frontal cortex lipid rafts from Parkinson's disease and incidental Parkinson's disease. Mol. Med. 17:1107–1118.
89. Canerina-Amaro A, Pereda D, Diaz M, Rodriguez-Barreto D, Casañas-Sánchez V, Heffer M, Garcia-Esparcia P, Ferrer I, Puertas-Avendaño R, Marin R (2019) Differential aggregation and phosphorylation of alpha synuclein in membrane compartments associated with Parkinson disease. Front. Neurosci. 13:1–21.
90. Phillips AS, Gomes AF, Kalapothakis JMD, Gillam JE, Gasparavicius J, Gozzo FC, Kunath T, MacPhee C, Barran PE (2015) Conformational dynamics of α-synuclein: Insights from mass spectrometry. Analyst 140:3070–3081.
91. Martin Ester, Hans-Peter Kriegel, Jorrg Sander XX A Density-Based Algorithm for Discovering Clusters in Large Spatial Databases with Noise. Proc. Second Int. Conf. Knowl. Discov. Data Min. KDD-96:226–231.